Uniformity Correction for SPECT Using a Mapped Cobalt-57 Sheet Source

Bernard E. Oppenheim and C. Robert Appledorn

Department of Radiology, Indiana University School of Medicine, Indianapolis, Indiana

As little as 1% nonuniformity of the scintillation camera can produce disturbing artifacts in SPECT images. To correct for nonuniformity, acquired images must be divided by the flood-field image of a uniform sheet source. The refillable ^{99m}Tc sheet source requires meticulous preparation before each use, and is subject to spillage. We propose the use of a permanent ^{57}Co solid sheet source in conjunction with a map of the radioactivity distribution in the source. The flood-field image of the cobalt source is converted by the map into the equivalent of a flood-field image of an almost perfectly uniform source. An accurate and reproducible method is described for generating a map of the cobalt sheet source from images of it made in multiple positions with the scintillation camera. The mapping process is independent of sensitivity variations across the face of the camera.

J Nucl Med 26:409–415, 1985

Single photon emission computed tomography (SPECT) with a rotating scintillation camera places stringent requirements on camera uniformity. Rogers et al. (*1*) have shown through computer simulation that nonuniformity with a relative standard deviation (r.s.d.) of 1% can sometimes produce detectable artifacts in reconstructions containing 2.5×10^6 counts per slice. Our own simulations confirm this (Fig. 1).

The simulations imply that the camera with collimator should have a nonuniformity no greater than 1% r.s.d. To meet this requirement one must correct acquired images using a flood-field image of a large source containing uniformly distributed radioactivity. Unfortunately, any nonuniformities in the radioactivity distribution of the source will introduce artifacts similar to those obtained with an equivalently nonuniform camera. Uniformity requirements for the source are, in fact, even more stringent than those for the camera, since the flood-field image will contain statistical variation due to finite counts.

Refillable technetium-99m (^{99m}Tc) liquid sheet sources are widely used for generating flood-field images for SPECT uniformity correction, but good source uniformity requires meticulous preparation (*1–3*) and one must contend with the possibility of spillage and contamination. A solid cobalt-57 (^{57}Co) sheet source would be more convenient to use as it requires no preparation and is not subject to spillage, but source nonuniformity has generally been somewhat greater than 1% r.s.d. (*1,2*). This limitation could be overcome, however, if we had a map of the radioactivity distribution in the cobalt sheet source. We would then be able to correct a flood-field image of the source using the source map, and thus obtain an image which is equivalent to the flood-field image of an almost perfectly uniform source.

A map generated from a single image of the cobalt sheet source made with a scintillation camera would be unsatisfactory because it would incorporate the effects of camera nonuniformity. These effects can be removed if we image the source in a number of different positions along both the x-axis and the y-axis of the camera with adjacent positions separated by some fixed distance d. We can then consider the source and the camera to be subdivided into pixels of size d × d. Each pixel of the camera will image a group of adjacent pixels of the source, and the ratios of the counts for those pixels are measures of the ratios of the activity contained in those pixels of the source, *independent* of the sensitivity of the particular camera pixel doing the imaging. From these

Received Aug. 15, 1984; revision accepted Jan. 22, 1985.

For reprints contact: Bernard E. Oppenheim, MD, Dept. of Radiology, Indiana University School of Medicine, 1100 W. Michigan St., Indianapolis, IN 46223.

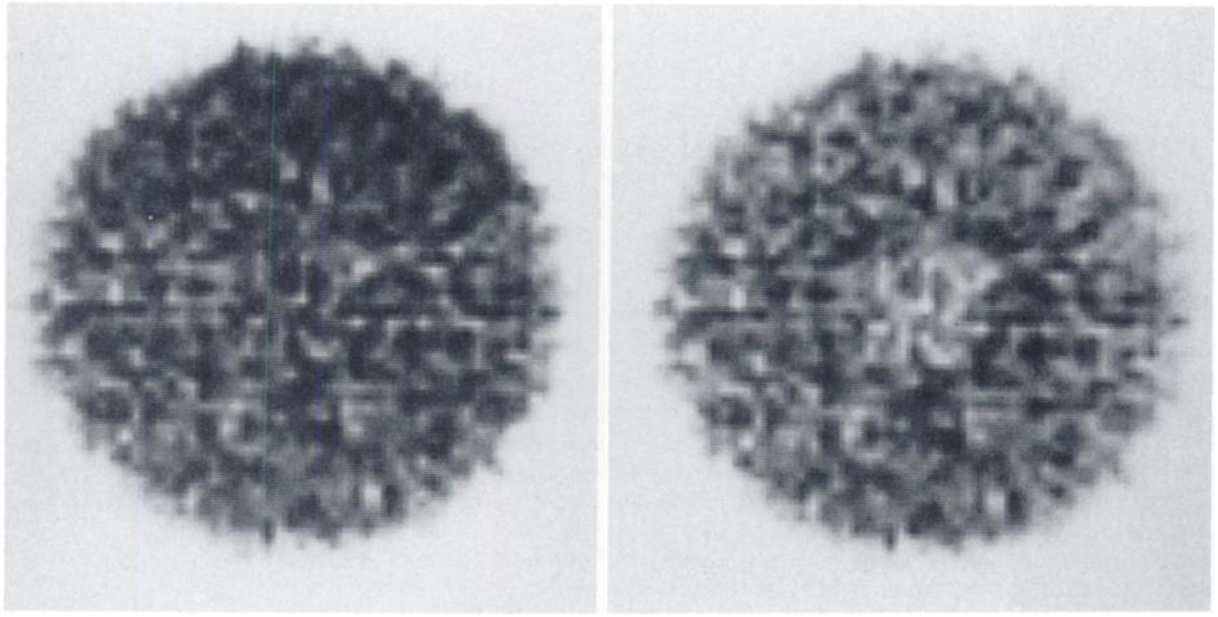

FIGURE 1
Simulation of effect of 1% r.s.d. nonuniformity of camera on reconstructed slice containing 2.5×10^6 total counts. A: Noisy data, uniform camera. B: Same data with 1% r.s.d. nonuniformity. Irregular central defect is present. Seven of 30 simulations had comparable artifacts

ratios one can construct a map of the source through a series of algorithms described in the Appendix.

The procedure described in this report will permit mapping of a cobalt sheet source with a root-mean-square (r.m.s.) error of about 0.5%, based on computer simulations and two independent mappings of a source using two different scintillation camera heads.

MATERIALS AND METHODS

Computer simulations

The parameters that must be specified in the mapping procedure are the total number of counts to be detected, the number of source positions along each axis, and the pixel size (representing the distance between source positions). If the pixel size is chosen too small, the necessary positioning accuracy and counting requirements could not be met through manual positioning of the source; hence, a pixel size of 12 mm was chosen a priori as a size that would be practical to deal with in the actual experiment. Then a detector with an imaging area 40 cm in diam would be represented by a 31 × 31 array (the array has odd dimensions because the present method for mapping the source requires a central pixel).

Simulations were carried out for $30M$, $100M$, and $300M$ total counts and 3, 5, 7, 9, and 11 source positions per axis. The source activity distribution and the detector sensitivity distribution were represented by random values, normalized to an average value of 1, which were assigned to those pixels of a 31 × 31 array included within a circle 31.2 pixels in diam (the remaining pixels were assigned the value zero). Images were generated for each source position, in which the counts assigned to each pixel were generated from a Poisson random variable with mean value equal to the product of the source activity and detector sensitivity for that pixel, multiplied by the average counts per pixel. The source map was computed by the algorithms described in the Appendix, and its r.m.s. error, as compared with the actual source activity distribution, was determined. The procedure was repeated for 100 trials (25 trials for nine or 11 source positions).

Simulations were carried out in which 100 independent pairs of maps were generated using $214M$ total counts and nine positions per axis (the parameters used in the actual mapping experiment), and the r.m.s. error in each mapping and the r.m.s. difference in each pair of mappings were determined.

Source mapping

A 1.9 mCi ^{57}Co sheet source* was imaged for identical time in nine positions along the horizontal axis of the camera face, and in nine positions along the vertical axis, with a 12 mm separation between adjacent positions. Approximately 12 million counts were acquired in 20 min in each position, for a total of 214 million counts. Imaging was carried out using the red head of a dual headed camera† interfaced to a computer.‡ The procedure was repeated using the green head of the camera.

To achieve accurate positioning, horizontal and vertical lines were drawn on the source, and cross-marks were made corresponding to each position to which the source was to be moved.

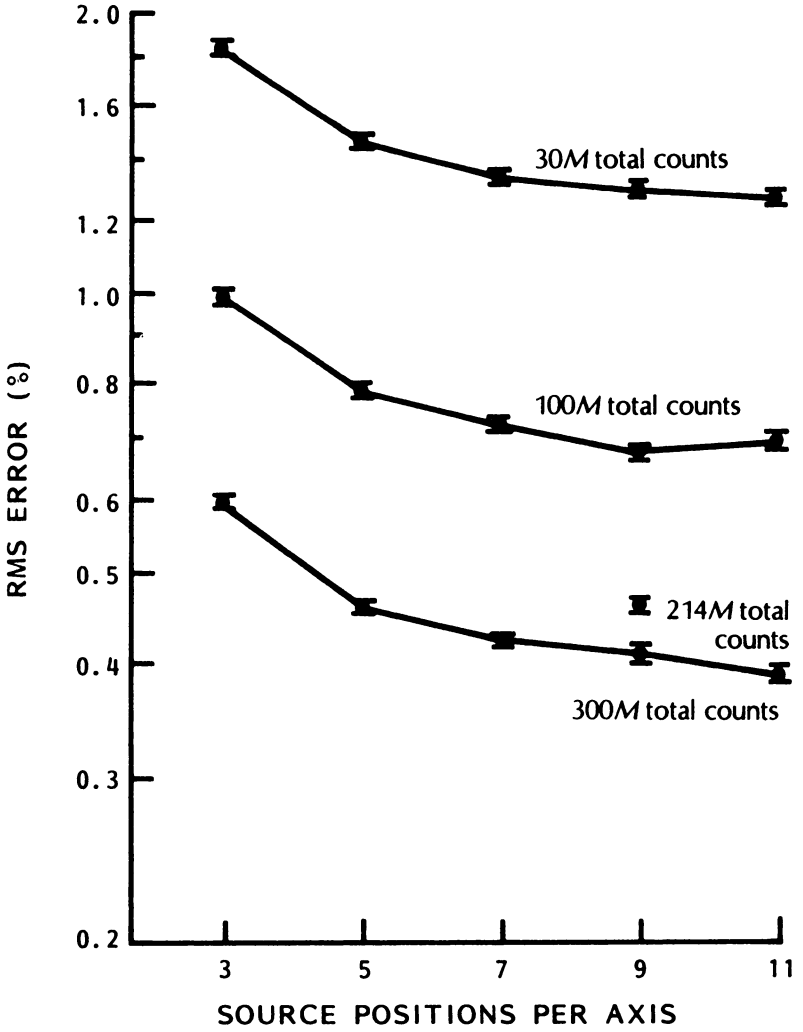

FIGURE 2
Percent r.m.s. error in simulated mapping of 31 × 31 source as function of total counts detected and number of source positions along each axis. Error decreases with increasing total counts, and with increasing source positions. For 214*M* total counts and nine positions per axis, corresponding to actual mapping carried out, predicted r.m.s. error is 0.46%

A string, taped at one end, was stretched precisely along the horizontal axis of the camera face, and a similar string was stretched precisely along the vertical axis. For movement of the source along the horizontal axis, the source was positioned so that the horizontal line on it coincided with the horizontal string, while one of the cross-marks coincided with the vertical string. Movement along the vertical axis was accomplished in a similar manner.

For calibration a four-quadrant bar phantom was positioned so that its axes coincided with the axes of the camera head, and was imaged using the cobalt source. It was then rotated 90° and imaged again. This was done with both the red and the green heads of the dual headed camera. From these images, combined with measurement of bar spacing in the phantoms, calibration factors were determined representing the coordinates of the physical center of the camera head and the scale for each axis.

The images of the source obtained with each head were centered, rescaled, and converted into 31 × 31 arrays of pixels, using the calibration factors. The ratio of the activity of each pixel of the source to that of each of its neighbors was determined. From these ratios a 31 × 31 map of the source was constructed, in which the central pixel was assigned an arbitrary value of 10,000 counts. The map was interpolated to 64 × 64 and then shifted and rescaled, by means of the calibration factors, to be of the correct size and location for an image made with the corresponding camera head. This procedure is described in detail in the Appendix.

A difference image was generated from the 31 × 31 maps for each camera head, and the r.m.s. difference in the maps was determined from that image.

RESULTS

Computer simulations

The results of the simulations are shown in Fig. 2. As might be expected, the r.m.s. error decreases with increasing total counts. It is also seen that for fixed total counts the error decreases as the number of source positions is increased, but the decrease is negligible beyond nine positions per axis. It was on the basis of these simulations that we chose to move the source to nine positions along each axis, and to collect in excess of 200 million total counts, as this should have permitted a mapping with an r.m.s. error of about 0.5%.

The simulations based on the parameters used in the actual mapping experiment (214*M* total counts, nine positions per axis) revealed an expected r.m.s. error in each mapping of

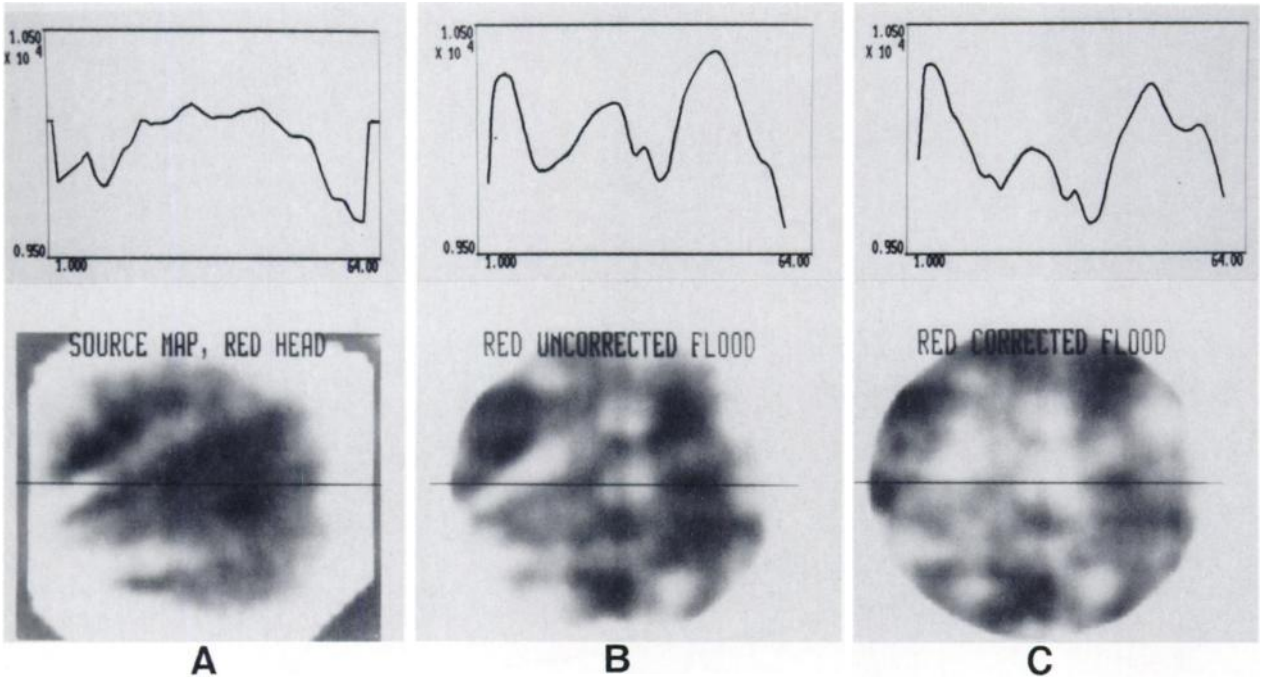

FIGURE 3
Mapping of cobalt source with red head of dual headed camera. Above each image is central profile on scale from 9,500 to 10,500 counts. A: 31 × 31 source map interpolated to 64 × 64, demonstrating multiple bands of increased and decreased activity. B: High count flood-field image made with source, demonstrating linear and circular defects. C: Flood-field image corrected with source map. Linear defects attributable to source have been mostly removed

0.46% (s.d. 0.08%, s.e.m. 0.006%), and an expected r.m.s. difference in the pair of mappings of 0.65% (s.d. 0.12%, s.e.m. 0.012%).

The choice of detector sensitivity distribution was found to have no effect on the results of these simulations, and the choice of source activity distribution was found to have only a minimal effect.

Source mapping

The source map obtained with the red head of the dual headed camera is shown in Fig. 3A, along with a central profile of counts in the map on a scale from 9,500 to 10,500 counts (the central profiles for other images are scaled similarly). There are several bands of alternating increased and decreased activity in the source, having about a 3 to 4% variation from peak to valley. Figure 3B is a high count, flood-field image of the source, made with the red head. This image contains both round defects due to nonuniform camera sensitivity and linear defects due to nonuniform radioactivity distribution in the source. Figure 3C is a corrected flood-field image obtained by dividing the uncorrected image (Fig. 3B) by the source map. The linear defects due to the source have been mostly removed.

The results of mapping the source with the green head of the dual headed camera are shown in Fig. 4. The map (Fig. 4A) is quite similar to the one obtained with the red head. In this instance, however, the camera was poorly tuned and the flood-field images, both uncorrected (Fig. 4B) and corrected by the source map (Fig. 4C), are very nonuniform.

The r.m.s. difference in the two 31 × 31 maps, relative to the average value of either map, was found to be 0.68%. A slight misregistration of the two maps was discovered, which was corrected by shifting the imputed physical center of the images obtained with the red camera head by 0.7 mm in the x-direction and 2.6 mm in the y-direction and recomputing the map for that head. This reduced the r.m.s. difference in the two maps to 0.66%. In comparison, the individual red and green 31 × 31 maps had nonuniformities of 1.91% r.s.d. and 2.03% r.s.d., respectively.

DISCUSSION

Camera nonuniformity as small as 1% r.s.d. can produce disturbing and misleading artifacts in SPECT images (*1*) (see Fig. 1). An artifact of this type generally appears as a central "hot spot" or "cold spot" in the image, although it may also take on the form of a concentric hot or cold ring (*2,4*). The amplitude of the artifact is related to the amplitude of the camera nonuniformity, but it depends more strongly on the distance r from the nonuniform region to the axis of rotation as detected by the camera, being maximum if the nonuniform region overlies the detected axis, and decreasing in proportion to $1/\sqrt{r}$ for regions at a distance from the axis (*2,5*). The on-axis nonuniformities produce the "hot" or "cold" spots, while the off-axis defects produce the rings, which are much less disturbing because of their lower amplitudes.

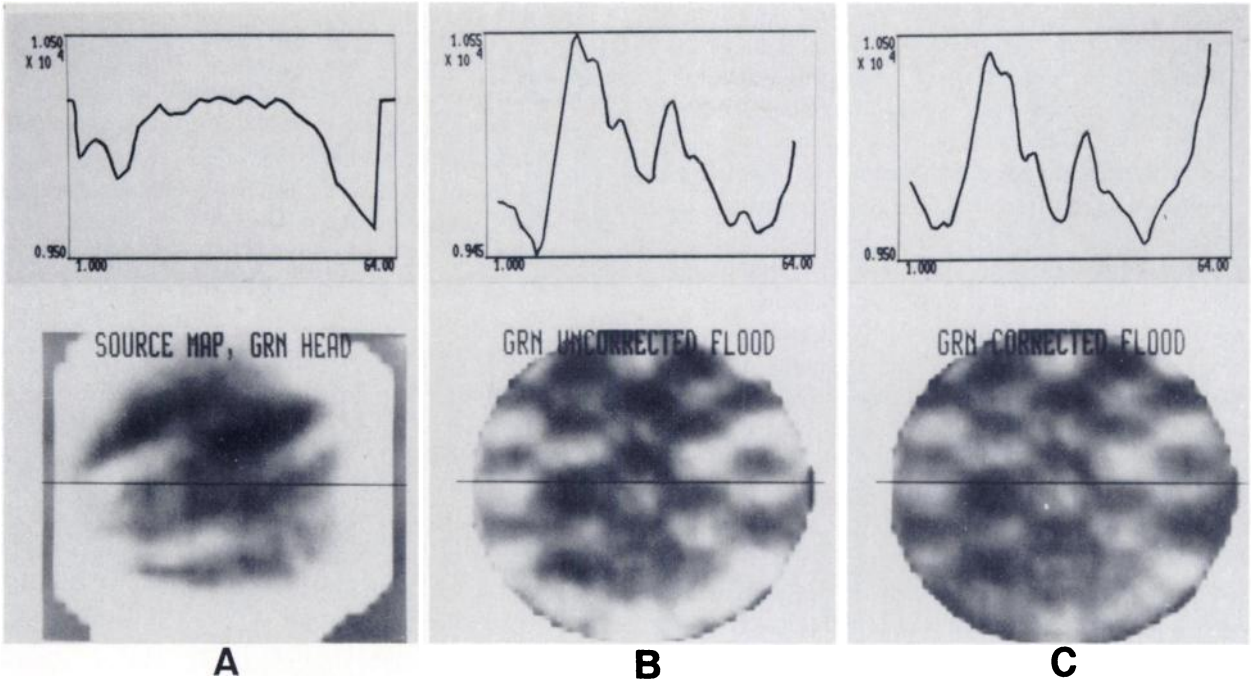

FIGURE 4
Mapping of cobalt source with green head of dual headed camera. A: Source map. B: Uncorrected flood-field image. C: Flood-field image corrected with source map. Map is quite similar to one obtained with red head, although camera is poorly tuned with very nonuniform sensitivity

Various measures of camera uniformity are in use, such as "integral" and "differential" uniformity proposed by the National Electrical Manufacturers Association (*6*), and the relative standard deviation (r.s.d.) measure used here and by Rogers et al. (*1*). None of these measures is indicative of the magnitudes of the artifacts produced in SPECT images by nonuniformities, since none takes into account the positions of the nonuniformities relative to the axis of rotation. We prefer the r.s.d. measure because it facilitates simulation and intercomparison of results.

Since camera nonuniformities will generally be greater than 1% r.s.d., some method of correction is required. Todd-Pokropek (*7*) has devised an image filter that will suppress uniformity artifacts in SPECT images by taking advantage of their concentric nature, but will also suppress lesions that are centrally located or have a concentric component. It is preferable to directly attack the cause of the artifact by acquiring a flood-field image of a uniform sheet source and correcting the images produced by the camera using this image. While a refillable ^{99m}Tc sheet source is generally recommended for this purpose (*1*,*2*) we believe that a ^{57}Co solid sheet source, used in conjunction with a map of the source, is preferable because it requires no preparation before each use, is easily handled and stored, and is not subject to spillage. Furthermore, its uniformity is constant, demonstrable, and will be equivalent to about 0.5% r.s.d. if flood-field images are corrected by a map of that accuracy, while the uniformity of the refillable ^{99m}Tc sheet source is uncertain and may vary with each preparation.

Mapping of the cobalt source is recommended even in those instances in which the manufacturer certifies the source to be uniform within 1% r.s.d. The source that we used was certified to have a uniformity of 0.8% r.s.d. over its entire active area, yet the two maps that we generated had uniformities of 1.9% r.s.d. and 2.0% r.s.d.

The source was mapped by imaging it in multiple positions with the scintillation camera. The alternative approach of scanning the source with a rectilinear scanner was rejected because the map thus obtained would be difficult to apply to images made with a camera, and would be of questionable validity because of the different depths of field of scanner and camera collimators. In our method, each pixel of the camera functions like a separate detector which is scanning a region of the source. The sensitivity of that detector does not affect the ratios of counts detected across the scanned region, from which the source map is generated. It is for this reason that very similar maps were generated using the red head and the green head of the dual headed camera, even though these two heads had very different sensitivity distributions (Figs. 3 and 4).

Mapping could have been accomplished by imaging the source in as few as two positions along each axis, as that would have provided a single measure of the ratio of activity for every pair of adjacent pixels in the source.

There is a statistical error in the estimate of each ratio, however, and these errors accumulate as the ratios are multiplied together by the mapping algorithm. By imaging the source in multiple positions along each axis, multiple estimates of each ratio are obtained, which reduces the statistical error even though the total number of counts detected remains fixed, as demonstrated in Fig. 2.

The bar phantom images proved unsatisfactory for determining calibration factors, and we found it necessary to adjust the coordinates of the center of the red head by a fraction of a pixel to bring the maps for the two heads into registration. We would now recommend that calibration factors be determined from images of small point sources placed at the center of the camera head and on each axis 10 cm either side of the center.

The r.m.s. difference in the 31 × 31 maps made with the red and green camera heads, after registration, was 0.66%. In comparison the r.m.s. difference in two maps, as predicted from simulations in which the only source of error was the uncertainty due to finite counting statistics, was 0.65% ± 0.12% (mean ± 1 s.d.). Thus the component of error due to causes other than finite counting statistics, such as spatial nonlinearity of the cameras (*8*) and source mispositioning, must be small. Hence, one may consider the r.m.s. error of 0.46% ± 0.08% (mean ± 1 s.d.) obtained through simulated mapping of a single source to be a good estimate of the actual mapping error.

Manual positioning of the source for mapping is quite tedious. The data collection took 8 hr per head for a 1.9 mCi source. Fortunately, the mapping only has to be carried out once, since the activity distribution should remain constant in the absence of damage to the source. It would be preferable, however, to have a device for automatic positioning of the source, since this would simplify the mapping procedure and would permit higher count acquisition and finer source movement. We are currently developing such a device.

A mapped cobalt sheet source could be used with any camera for uniformity correction. The source must be accurately centered and aligned with the axes of the camera head (stretched strings, as described in this report, are recommended for this purpose), and at least 30 million counts must be acquired as a 64 × 64 flood-field image (*1*). The coordinates of the center of the camera and the scale factors for each axis are determined from a calibration image of appropriately placed point sources. The source map, which has been stored in the computer, is rescaled in size and shifted to coincide with the flood-field image. The latter is divided by the source map to produce a corrected flood-field image,which is subsequently used for uniformity correction of images acquired with that camera. Smoothing may be applied to the corrected flood-field image provided that comparable smoothing is applied to the acquired images (*1*).

CONCLUSIONS

We have demonstrated a method for mapping the radioactivity distribution in a ^{57}Co sheet source. This map can be used to convert a flood-field image of the cobalt source into the equivalent of a flood-field image of an almost perfectly uniform source. The method is reproducible, as demonstrated by the close similarity of maps generated from two different scintillation camera heads, even though one of the heads was badly out of tune. The mapping procedure, implemented as described, has an expected r.m.s. error of about 0.5%. The procedure is tedious and requires great care, but only has to be done once for each source.

A mapped cobalt source could be used for uniformity correction of any camera. It would be easier and more convenient to use than a ^{99m}Tc liquid-filled source, since it would require no preparation, and with careful source alignment it should provide a highly accurate correction.

FOOTNOTES

* Amersham International Limited.
† Siemens Rotacamera.
‡ Medical Data Systems A² Clinical Imaging System.

APPENDIX

The activity distribution of the cobalt sheet source is determined in the following manner:

The source is imaged in p positions (designated by m = $-(p-1)/2, \ldots, 0, \ldots, (p-1)/2$) along the horizontal and vertical axes of the detector (camera head), where p is odd. The source and detector are concentric in position m = 0 along each axis. The distance between adjacent source positions is d. The source and detector are considered to be divided into an n × n array (n odd) of pixels S(i,j) and D(i,j) of size d × d, with the horizontal and vertical axes of the source and detector passing through the center of the centrally located pixels S(0,0) and D(0,0).

For the source in horizontal position m, we define $C_h(i,j,m)$ as the log of counts detected in pixel D(i+m,j), for an arbitrarily fixed counting time, these counts originating in pixel S(i,j). $C_h(i,j,m)$ is considered to be undefined if either S(i,j) is not entirely included within the physical boundaries of the source, or D(i+m,j) is not entirely within the useful field of view of the detector.

We define

$$R_h(i,j,m_a,m_b) = C_h(i,j,m_a) - C_h(i + m_a - m_b,j,m_b)$$
when both terms are defined
= 0 when either term is undefined

$$\hat{R}_h(i,j) = \frac{\sum_m R_h(i,j,m,m+1)}{\text{number of nonzero terms}}$$

$$H(i,j) = \hat{R}_h(i,j) \text{ for } i > 0$$
$$= -\hat{R}_h(i+1,j) \text{ for } i < 0$$
$$\text{undefined for } i = 0.$$

Here $R_h(i,j,m_a,m_b)$ represents the log of the ratio of counts in S(i,j) to counts in $S(i + m_a - m_b,j)$ as detected by the single pixel $D(i + m_a,j)$, and hence is independent of the sensitivity of that pixel of the detector; $\hat{R}_h(i,j)$ is the average log ratio of counts in S(i,j) to counts in $S(i - 1,j)$, as counted by multiple pixels in the detector, and is an estimator of the log ratio of activity of S(i,j) to $S(i - 1,j)$; and H(i,j) is the estimated log ratio of the activity of S(i,j) to the activity of the horizontally adjacent pixel that is closer to the vertical axis of the source.

We similarly define $C_v(i,j,m)$ as the log of counts detected in pixel $D(i,j + m)$ for the source in position m along the vertical axis of the detector, these counts originating in pixel S(i,j) of the source.

We also define

$$R_v(i,j,m_a,m_b) = C_v(i,j,m_a) - C_v(i,j + m_a - m_b,m_b)$$

$$\hat{R}_v(i,j) = \frac{\sum_m R_v(i,j,m,m+1)}{\text{number of nonzero terms}}$$

$$V(i,j) = \hat{R}_v(i,j) \text{ for } j > 0$$
$$= -\hat{R}_v(i,j+1) \text{ for } j < 0$$
$$\text{undefined for } j = 0.$$

We also define i_p, j_p, and k_p, the "previous" values of the indices i, j, and k, as the integers closer to zero;

$$i_p = i - 1 \text{ for } i > 0$$
$$i_p = i + 1 \text{ for } i < 0$$

and similarly for j_p and k_p.

Initially each of the input images is centered, rescaled, and reformatted into an n × n array (n is odd) of values representing the log of counts detected in each pixel D(i,j) of the detector. These values correspond to C_h or C_v, and are set to $-32K$ (= undefined) whenever a pixel is not entirely within the source or the useful field of view of the detector. Each image but the first for each axis is subtracted from the previous image to yield p − 1 difference images for each axis, representing $R_h(i,j,m,m+1)$ and $R_v(i,j,m,m+1)$ for $m = -(p-1)/2$ to $(p-3)/2$. The value of R_h or R_v is set to zero when a corresponding value of C_h or C_v is undefined. The images are aligned by shifting each one by −m pixels, and for each position (i,j) the average of the nonzero terms is determined, to produce $\hat{R}_h(i,j)$ and $\hat{R}_v(i,j)$. These arrays are converted into the arrays H(i,j) and V(i,j), where H(i,j) represents the estimated log ratio of the activity of pixel S(i,j) to the activity of pixel $S(i_p,j)$, and V(i,j) represents the estimated log ratio of the activity of pixel S(i,j) to the activity of pixel $S(i,j_p)$.

We define A(i,j) as the n × n array representing the estimated log ratio of the activity of pixel S(i,j) to the activity of the central pixel S(0,0). This is computed recursively from the log ratio values H(i,j) and V(i,j) by adding rings of pixels to the central pixel until the n × n array is filled in, by the following formulas:

$$A(0,0) = 0$$
For $k = \pm 1, \pm 2, \ldots, \pm(n-1)/2$:

$$A(0,k) = A(0,k_p) + V(0,k)$$

$$A(i,k) = [A(i,k_p) + V(i,k)]/2 + [A(i_p,k) + H(i,k)]/2$$
for $i = \pm 1, \pm 2, \ldots, \pm(k-1)$

$$A(k,0) = A(k_p,0) + H(k,0)$$

$$A(k,j) = [A(k_p,j) + H(k,j)]/2 + [A(k,j_p) + V(k,j)]/2$$
for $j = \pm 1, \pm 2, \ldots, \pm(k-1)$

$$A(i,j) = [A(i,j_p) + V(i,j)]/2 + [A(i_p,j) + H(i,j)]/2$$
for $i = \pm k$ and $j = \pm k$.

Here the values for the on-axis pixels of the k^{th} ring are represented by A(0,k) and A(k,0), the values for the off-axis pixels of that ring are represented by A(i,k) and A(k,j), and the values for the four corner pixels of the ring are represented by A(i,j), for the indicated values of the indices i and j.

The estimated n × n source activity distribution, scaled upward so that the central pixel has 10,000 counts, is given by antilog [A(i,j) + 4]. This array must be resampled, with shifting of the origin and rescaling of the coordinate axes, to correspond to the 64 × 64 image of the source made with a specific camera.

REFERENCES

1. Rogers WL, Clinthorne NH, Harkness BA, et al: Field-flood requirements for emission computed tomography with an Anger camera. *J Nucl Med* 23:162-168, 1982
2. Axelsson B, Israelsson A, Larsson S: Non-uniformity induced artifacts in single-photon emission computed tomography. *Acta Radiol Oncol* 22:215-224, 1983
3. English RJ, Polak JF, Holman BL: An iterative method for verifying systematic nonuniformities in refillable flood sources. *J Nucl Med Technol* 12:7-9, 1984
4. Jaszczak RJ, Coleman RE: Selected processing techniques for scintillation camera based SPECT systems. In *Single Photon Emission Computed Tomography and Other Selected Computer Topics*, Sorenson JA, ed. New York, Society of Nuclear Medicine, 1980, pp 45-59
5. Shepp LA, Stein JA: Simulated reconstruction artifacts in computerized x-ray tomography. In *Reconstruction Tomography in Diagnostic Radiology and Nuclear Medicine*, Ter-Pogossian MM, Phelps ME, Brownell GL, et al., eds. Baltimore, University Park Press, 1977, pp 33-48
6. *Performance Measurements of Scintillation Cameras.* Standards Publication/No. NU1-1980. Washington, D.C., NEMA, 1980
7. Todd-Pokropek AE, Jarritt PH: The noise characteristics of SPECT systems. In *Computed Emission Tomography*, Ell PJ, Holman BL, eds. New York, Oxford University Press, 1982, pp 361-389
8. Todd-Pokropek AE, Erbsmann F, Soussaline F: The non-uniformity of imaging devices and its impact in quantitative studies. In *Medical Radionuclide Imaging*, Vol. 1, Vienna, IAEA, 1977, pp 67-84